Dynamics of magnetic particles near a surface : model and experiments on field-induced disaggregation

Dynamics of magnetic particles near a surface: Model and experiments on field-induced disaggregation

A. van Reenen,[1,3] Y. Gao,[2,3] A. M. de Jong,[1,3] M. A. Hulsen,[2] J. M. J. den Toonder,[2,3] and M. W. J. Prins[1,3,4,*]

[1]*Department of Applied Physics, Eindhoven University of Technology, Eindhoven, The Netherlands*

[2]*Department of Mechanical Engineering, Eindhoven University of Technology, Eindhoven, The Netherlands*

[3]*Institute for Complex Molecular Systems (ICMS), Eindhoven, The Netherlands*

[4]*Philips Research, Eindhoven, The Netherlands*

(Received 31 December 2013; revised manuscript received 5 March 2014; published 22 April 2014)

Magnetic particles are widely used in biological research and bioanalytical applications. As the corresponding tools are progressively being miniaturized and integrated, the understanding of particle dynamics and the control of particles down to the level of single particles become important. Here, we describe a numerical model to simulate the dynamic behavior of ensembles of magnetic particles, taking account of magnetic interparticle interactions, interactions with the liquid medium and solid surfaces, as well as thermal diffusive motion of the particles. The model is verified using experimental data of magnetic field-induced disaggregation of magnetic particle clusters near a physical surface, wherein the magnetic field properties, particle size, cluster size, and cluster geometry were varied. Furthermore, the model clarifies how the cluster configuration, cluster alignment, magnitude of the field gradient, and the field repetition rate play a role in the particle disaggregation process. The simulation model will be very useful for further *in silico* studies on magnetic particle dynamics in biotechnological tools.

DOI: 10.1103/PhysRevE.89.042306 PACS number(s): 83.10.Mj, 87.85.fk, 75.75.Jn, 02.60.−x

I. INTRODUCTION

Magnetic particles are widely applied in biosciences and *in vitro* diagnostics, mainly because such particles can be manipulated and interrogated by magnetic fields without perturbing the biological matter under study [1–7]. To obtain a high total effective surface area for biological binding and processing, the assays are always performed with ensembles consisting of many individual magnetic particles. With the advent of novel experimental techniques to actuate and detect magnetic particles [3,4,8–12] on the level of ensembles as well as on the level of individual particles and with the advent of corresponding miniaturized microfluidic devices [3,4,10,13,14], the need appears to understand and predict the behavior of magnetic particles in variable configurations. Yet it is difficult to model and predict the dynamics of particle ensembles because the behavior of the particle ensemble is not simply an extrapolation of the behavior of single particles due to the strong magnetic interactions between the particles [15], the hydrodynamic interactions between the particles [15,16], and the interactions between the particles and microdevice surfaces [4,8,17]. To avoid tedious experimentation and trial-and-error studies, it is important to develop modeling tools for *in silico* studies of the behavior of particles in time-varying magnetic fields and complex device geometries.

Here, we propose a model and a numerical approach to simulate magnetic particle dynamics at a fundamental level, see Fig. 1. The model integrates the known basic interactions that have already been studied separately, namely, Brownian motion [18], magnetic gradient forces [19,20], magnetic dipole-dipole interactions [4,21], and particle surface interactions [4,8,18]. To evaluate the proposed numerical model, we apply it to simulate a recently reported method by which clusters of magnetic particles can be disaggregated using magnetic fields [8]. The disaggregation method is based on magnetically attracting particles to a surface while inducing repulsive magnetic dipole-dipole interactions. Experimental data show that clusters consisting of tens of particles can be disaggregated in a short time. In this study, we compare the experimental data to simulated data, and we use the numerical model to study the influence of underlying parameters, such as the cluster configuration and the particle size. In this way, a fundamental understanding of field-based disaggregation is obtained, and criteria are identified for optimal functional performance. Finally, we discuss how the simulation of multi-particle dynamics can be broadly applied for the development of magnetic particle-based biotechnological tools.

II. THEORETICAL CONSIDERATIONS

Ensembles of magnetically actuated magnetic particles were numerically simulated with Brownian dynamics using MATLAB (MathWorks). The force on each Brownian particle consists of three terms: (i) a friction force which tends to decrease the energy of the particle, (ii) a random (Brownian motion) force which increases the energy of the particle, and (iii) a systematic force due to the interaction potential energy between Brownian particles plus any external forces [22]. The Brownian dynamics simulation [22,23] of an N-particle system involves integrating the following Langevin equation:

$$\frac{\partial}{\partial t}\mathbf{r} = \boldsymbol{\mu}\cdot\mathbf{F}_{\text{net}}(t) + k_B T\,\nabla\cdot\boldsymbol{\mu} + \mathbf{v}^{\text{ran}}(t), \tag{1}$$

where $\mathbf{r}$, $\mathbf{F}_{\text{net}}$, and $\mathbf{v}^{\text{ran}}$, respectively, are the vectors containing the $3N$ coordinates of the particle positions, the forces acting on the particles, and the random velocity contribution of the particles due to Brownian motion. Furthermore, $\boldsymbol{\mu}$ is the $3N \times 3N$ translational mobility tensor, containing 3×3 blocks $\boldsymbol{\mu}_{ij}$ with $i, j = 1 \cdots N$. The tensor $\boldsymbol{\mu}_{ij}$ is the mobility matrix

*Corresponding author: m.w.j.prins@tue.nl

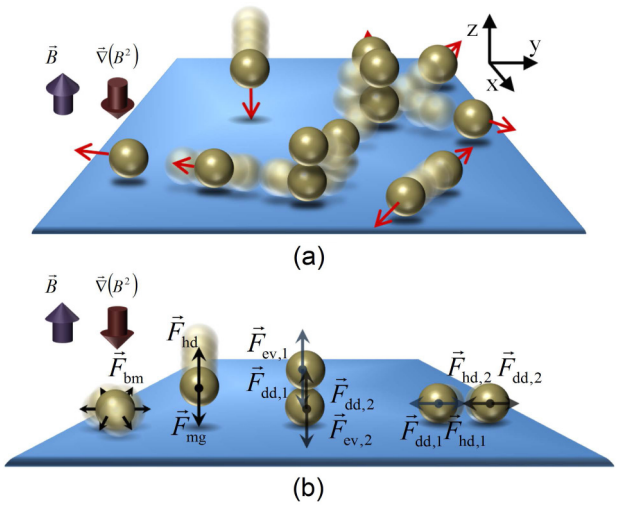

FIG. 1. (Color online) Overview of interactions of the magnetic particles. (a) Due to magnetic fields and magnetic field gradients, magnetic particles show dynamic behavior, interacting with the liquid, physical boundaries, and other particles. (b) Magnetic particles undergo thermal collision forces (i.e., exhibit Brownian motion), gravity, hydrodynamic interactions, and magnetic forces due to magnetic gradients and magnetic dipole-dipole interactions, which can be attractive or repulsive. The latter interaction has been exploited to disaggregate magnetic particle clusters [8].

approximated by the Rotne-Prager-Blake tensor [24]. In particular, this tensor accounts for the hydrodynamic interactions of particles with other particles and the surface [25–27]; for the explicit entries, see, for example, von Hansen *et al.* [24]. The blocks $\boldsymbol{\mu}_{ii}$ correspond to the self-mobilities of the particles and are diagonal matrices, whereas the other blocks $\boldsymbol{\mu}_{ij}$ with $i \neq j$ correspond to the hydrodynamic interactions between particles i and j. Note that the mobility tensor relates to the diffusion tensor via $\mathbf{D} = k_B T \cdot \boldsymbol{\mu}$, with $k_B T$ being the thermal energy. Lastly, the second term on the right-hand side of Eq. (1) compensates for the spatial variation in the particle mobility due to the Brownian motion [24,28].

Next, we describe expressions for the basic physical forces in the system, namely, magnetic dipole-dipole interactions, magnetic gradient forces, excluded volume forces, and random thermal excitations (Brownian motion). The expressions are adapted to the process of magnetic field-based disaggregation of magnetic particles as sketched in Fig. 1.

In an external magnetic field, $\mathbf{H}$ superparamagnetic particles become magnetized and obtain a magnetic moment: $\mathbf{m} = V\chi\mathbf{H}$, which depends on the volume V and the magnetic susceptibility of the particle χ. In case multiple N particles are present, the magnetic dipole-dipole interaction force $\mathbf{F}_{\mathrm{dd},i}$, acting on particle i, is given by [15,29]

$$\mathbf{F}_{\mathrm{dd},i} = \frac{3\mu_0}{4\pi} \sum_{\substack{j=1 \\ j\neq 1}}^{N} \frac{m_i m_j}{r_{ij}^4} \{[1 - 5(\hat{\mathbf{m}} \cdot \hat{\mathbf{r}}_{ij})^2]\hat{\mathbf{r}}_{ij} + 2(\hat{\mathbf{m}} \cdot \hat{\mathbf{r}}_{ij})\hat{\mathbf{m}}\}, \tag{2}$$

where m_i is the dipole moment of the ith particle; $\hat{\mathbf{m}}$ is the unit vector of the magnetic moment, which is assumed to be aligned with the external field $\mathbf{H}$; r_{ij} is the distance between the centers of the ith and jth particles, i.e., $r_{ij} = r_i - r_j$; and $\hat{\mathbf{r}}_{ij}$ is its corresponding unit vector. Here, we neglect the minor influence of other particles on the magnetic field. Furthermore, we neglect any effects of the field gradient on the magnetic dipole-dipole interactions because, in our experiments, the applied field gradients are small (few T/m) and the corresponding variation in the field in the near-surface region is much less than 1%. Furthermore, in our model, a physical surface is assumed at $z = 0$. Both a magnetic field gradient that is oriented towards the physical surface and gravity result in an additional downward force on each particle,

$$\mathbf{F}_{\mathrm{down},i} = \mathbf{F}_{\mathrm{mg},i} + \mathbf{F}_{\mathrm{buoyancy}} = \frac{V\mu_0\chi}{2} \frac{\partial H^2}{\partial z} \hat{\mathbf{e}}_z - V(\rho_{\mathrm{particle}} - \rho_{\mathrm{medium}}) g \, \hat{\mathbf{e}}_z, \tag{3}$$

with ρ being the volumetric mass density and g being the gravitational constant. In experiments, the gradient forces are generally much larger than the gravitational forces (see Supplemental Material [30]). An important advantage of gradient forces is that their magnitude and direction with respect to the surface can be controlled by the magnetic system.

To prevent the particles from crossing the physical boundary of the surface, reflecting boundary conditions were assumed. To model the hard core interactions between particles, excluded volume force formulations [15,29] are implemented. The excluded volume force is formulated such that: (i) upon overlap of the particles, a repulsive force is exerted which increases exponentially for increased overlap; and (ii) if the particles are not touching each other $r_{ij} > 2R$, the force is negligible with respect to other acting forces. Mathematically, the excluded volume force between the particles is formulated as [31]

$$\mathbf{F}_{\mathrm{ev},i} = 2\frac{3\mu_0}{4\pi(2R)^4} \sum_{\substack{j=1 \\ j\neq i}}^{N} m_i m_j \exp\left[-\xi\left(\frac{r_{ij}}{2R} - 1\right)\right] \hat{\mathbf{r}}_{ij}. \tag{4}$$

Here, R is the particle radius. The parameter ξ determines at what strength this force acts at varying distances. We find that, for $\xi = 3000$, the excluded volume force has a negligible effect on the computed particle movement in case particles are not in contact as explained in more detail in the Supplemental Material [30]. As we simulate the particle behavior always in the presence of magnetic fields, vanishing excluded volume forces for zero field strengths do not occur. Alternatively, excluded volume forces can be formulated as a Lennard-Jones potential [24].

Lastly, the random thermal motion of the particles follows from the fluctuation-dissipation theorem [22,24,28],

$$\left\langle \Delta\mathbf{r}_i^{\mathrm{ran}}(t) \Delta\mathbf{r}_j^{\mathrm{ran}}(t) \right\rangle = 2k_B T \boldsymbol{\mu}_{ij} \delta t. \tag{5}$$

To obtain the random displacement $\Delta\mathbf{r}^{\mathrm{ran}}$ for each particle, several mathematical approaches have been developed [23] of which we use the exact, but time-demanding, Cholesky decomposition. First, it is considered that the random displacement vector at any particular time and configuration of particles is equal to [23]

$$\Delta\mathbf{r}^{\mathrm{ran}} = \sqrt{2}\mathbf{B} \cdot d\mathbf{w}, \tag{6}$$

with $d\mathbf{w}$ as a vector with length $3N$ containing random values picked from a Gaussian distribution with zero mean and a variance equal to the (small) numerical time step δt and $\mathbf{B}$ as a $3N \times 3N$ matrix which results from the factorization of the diffusion tensor $\mathbf{D} = k_B T \cdot \boldsymbol{\mu}$ as required by the fluctuation-dissipation theorem,

$$\mathbf{D} = \mathbf{B} \cdot \mathbf{B}^T. \tag{7}$$

Any matrix $\mathbf{B}$ that satisfies Eq. (7) can be used in Eq. (6). So, we apply a Cholesky decomposition of $\mathbf{D}$ to obtain an upper triangular matrix $\mathbf{C}$, that satisfies Eq. (7): $\mathbf{D} = \mathbf{C} \cdot \mathbf{C}^T$ [23].

Based on these considerations, we integrate Eq. (1) with $\mathbf{F}_{\text{net}} = \mathbf{F}_{\text{dd}} + \mathbf{F}_{\text{down}} + \mathbf{F}_{\text{ev}}$ to compute the trajectories of all particles. In particular, a forward Euler method was applied using numerical time steps of $\delta t = 10^{-6}$ s. As discussed in the Supplemental Material [30], it was found that the size of δt was sufficiently small to keep computational errors well below 0.1% relative error in position at 0.5 s of simulated time.

III. MATERIALS AND METHODS

Experimentally, to generate magnetic fields in all directions, an octopolar electromagnet was used which was described earlier [31]. In short, the magnetic system consists of eight individually steered electromagnets together with eight soft-iron (ARMCO) poles connected by soft-iron frames. In the center of the magnetic setup, a fluid cell is positioned which contains the particles. Besides control over the field orientation, the strength and orientation of the field gradient can also be varied but to a lesser extent. For example, to obtain a field gradient oriented in the $-z$ direction, the two electromagnets, which are positioned at the bottom, are powered [8].

In experiments, superparamagnetic particles (2.8 μm diameter, Dynal M-270 COOH) were suspended in a fluid cell containing phosphate buffered saline with 1 mg/ml bovine serum albumin to reduce nonspecific adhesion of particles to each other and to the walls of the fluid chamber. The fluid cell consists of two glass cover slides, separated by 120 μm thick SecureSeal spacers (Grace BIO-LABS, Inc.) that contain a 9 mm diameter hole. The fluid cell was placed in the center of the magnet setup and under a microscope (Leica Microsystems DM6000). Images were recorded using a MotionPro X3 high speed camera. Custom particle center-tracking software based on cross correlation was used to determine the particle trajectories in the xy plane.

IV. RESULTS AND DISCUSSION

A. Separation dynamics of two-particle clusters

First, we experimentally recorded the response of two-particle clusters (2.8 μm diameter) on a surface after applying a magnetic field oriented perpendicular to the surface. From top-view images [see Fig. 2(c)], the in-plane center-to-center distance was determined over time as shown in Fig. 2(e). Strong nonlinear behavior was observed which corresponds to the reciprocal dependence of the magnetic dipole-dipole interaction force on the fourth power of the distance between the dipoles [see Eq. (2)]. At short distances, the response of the different particle pairs is similar and shows no significant

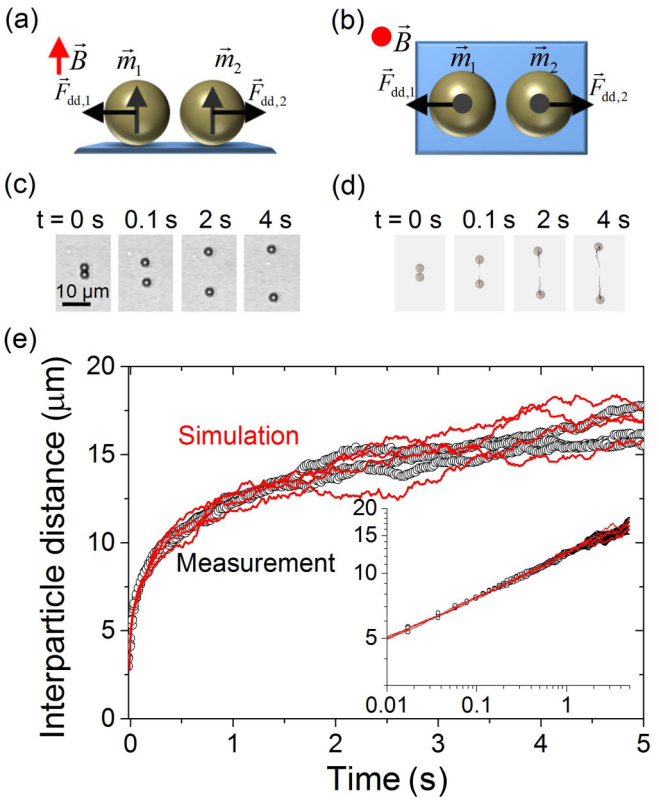

FIG. 2. (Color online) Measured and simulated disaggregations of a two-particle cluster at a physical surface in an aqueous medium. Schematic (a) side view and (b) top view are shown indicating the vectors corresponding to the magnetic field, magnetic moments, and the magnetic dipole-dipole forces. (c) Measured top-view images at different times ($\mathbf{B} = 15\,\text{mT}\,\hat{\mathbf{e}}_z$; $\nabla\mathbf{B} = -3.2\,T/\text{m}\,\hat{\mathbf{e}}_z$). (d) Simulated top-view images at different times. (e) In-plane center-to-center distance between the particles as obtained from the top-view experimental (black open circles) and simulated (red lines) data. Measurements were repeated on the same particle pair. The inset shows a log-log plot of the same data.

fluctuations in the distance. At longer distances, fluctuations become stronger, and we attribute this to the Brownian motion of the particles, which becomes more pronounced as the repulsive magnetic force has weakened.

Using the numerical approach as described, we simulated the response of two-particle clusters with similar properties; the particle properties were obtained from vibrating sample magnetometer data [31,32], and the properties of the magnetic fields were characterized from COMSOL simulations and Hall-probe measurements [8]. From the numerical data, the in-plane [top view, see Fig. 2(d)] interparticle distance was determined, which is shown in Fig. 2(e) for several simulations. As can be seen, the simulated interparticle distance shows exactly the same characteristics over time as was found in the experiments. Correspondence between simulation (with a similar method) and experiment was also found earlier for the breaking and reformation behavior of magnetic particle chains in a rotating magnetic field [31]. We, therefore, conclude that the used numerical method is an accurate tool to study the disaggregation behavior of magnetic particle clusters in more detail as we show next.

B. Parameters influencing the separation probability

The separation dynamics of two-particle clusters was studied for different parameters. First, we varied the orientation of the two-particle cluster with respect to the physical surface at the moment of application of the magnetic field. To this end, we define the angle of the longest axis of the two-particle cluster with the physical surface as the tilt angle α. We refer to the tilt angle at the time of application of the magnetic field as the initial tilt angle α_0. Due to Brownian motion of the particle cluster, the initial tilt angle will not always be zero, even when an in-plane magnetic field (with respect to the surface) is applied just before application of the out-of-plane magnetic field. For smaller particles, deviation from a zero initial tilt angle will be larger as compared to larger particles due to the larger diffusivity of smaller particles. Therefore, simulations were carried out in which the initial tilt angle was varied for two different particle sizes. In particular, we considered 2.8 μm particles (corresponding to Dynal M-270 particles) and 1.0 μm particles (corresponding to Dynal MyOne particles) which have an $\sim$9 times smaller magnetic moment [32].

In Fig. 3, both top and side views are shown for typical simulated particle trajectories. It is found that, for small initial tilt angles, particles irreversibly separate. For larger initial tilt angles, particles rejoin after initial separation and form vertical clusters, giving unsuccessful disaggregation. The driving force of this cluster reformation is the magnetic dipole-dipole interaction. Complete separation of the magnetic particles only occurs in case the relative distance vector [$\mathbf{r}_{ij}$, see Eq. (2)] between the magnetic moments $\mathbf{m}$ is orthogonal to the orientation of the magnetic moments. In case the relative distance vector deviates from being orthogonal to the magnetic moment ($\mathbf{m} \cdot \mathbf{r}_{ij} \neq 0$), the magnetic dipole-dipole interaction will lead to alignment of the two moments. Brownian motion generates variations in the direction of $\mathbf{r}_{ij}$, and therefore, additional forces are required to stabilize an orthogonal orientation of the particle clusters with respect to the external field. The presence of the surface and the field gradient towards the surface can stabilize such an orientation and can keep the interaction repulsive as particles are in a local energy minimum when both are in contact with the surface. This is also observed in Fig. 3; for a zero initial tilt angle, both particle types do not show cluster reformation.

For nonzero initial tilt angles, one of the particles is lifted initially while also moving away from the other particle. In case the initial tilt angle is small enough, the lifted particle eventually returns to the surface again due to the field gradient and then remains separated from the other particle. For higher angles, the lifted particle eventually returns to the other particle and reforms the cluster.

Comparing different particle sizes, the 3 μm particles stay closer to the surface after successful separation, i.e., the average distance from the surface is much smaller than the particle radius, whereas for the smaller 1 μm particles, the average distance from the physical surface is comparable to the particle radius. Comparing thermal energy to the potential energy due to the downward force ($\mathbf{F}_{\text{down}} = 0.26$ pN), we can estimate the distance of the particle surface from the planar surface within which a particle may be found with a probability of 0.9 (cf. the barometric height). For the 2.8 μm particles, this distance is estimated to be 0.05 μm, and for the 1.0 μm particles, it is 0.45 μm; these numbers are found to be roughly in agreement with our numerical results.

Since Brownian motion introduces statistical variability of the numerical outcome of a simulation at a certain initial tilt angle, we carried out 200 simulations per initial tilt angle and determined the probability of successful separation for both particle types. In the simulations, a downward force of $\mathbf{F}_{\text{down}} = 0.26$ pN was used. Each simulation was performed for 10 s as cluster reformation is found to occur typically in less than 1 s (see Ref. [30]).

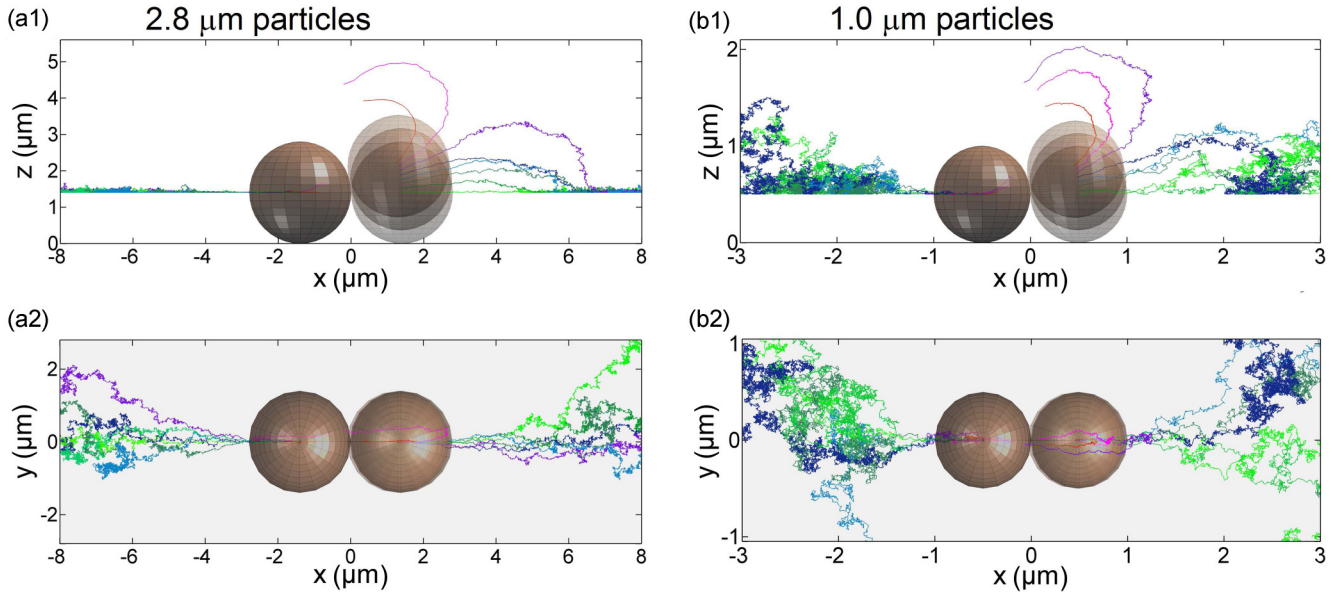

FIG. 3. (Color online) Computed particle trajectories at different initial tilt angles with respect to the surface. ($\mathbf{B} = 15\,\text{mT}\,\hat{\mathbf{e}}_z$; $\nabla\mathbf{B} = -2.8\,\text{T/m}\,\hat{\mathbf{e}}_z$) (a1) Side view and (a2) top view of simulations of 2.8 μm particles (M-270). (b1) Side view and (b2) top view of simulations of 1 μm particles (MyOne). The sketched spheres represent initial positions of the particles.

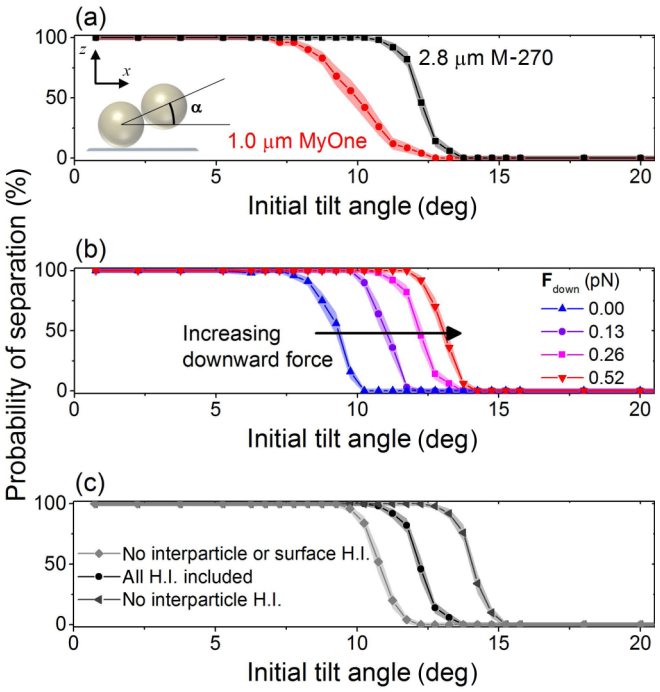

FIG. 4. (Color online) Computed probability of successful separation as a function of the initial tilt angle with respect to the surface. (a) Data for different particles using a downward force of $|\mathbf{F}_{\text{down}}| = 0.26$ pN. (b) Data for 2.8 μm sized particles (M-270) at different downward forces; i.e., combined magnetic gradient forces and buoyancy. (c) Comparison of data for 2.8 μm sized particles (M-270) in case the hydrodynamic interactions (H.I.s) between the particles and/or with the surface were excluded from the simulations. Each data point corresponds to the mean of 200 simulations. Particles that did not reform into a cluster within 10 s are counted as successful separations. The (small) standard error of the mean is represented by the shaded area around the data.

Figure 4(a) shows that smaller particles can reform clusters for a smaller range of initial tilt angles. Also, the transition from a 100% separation probability to a 0% separation probability is broader for smaller particles, which is explained by the higher diffusivity of smaller particles. Interestingly, for both particles, there is a nonzero range of initial tilt angles for which two-particle clusters can be separated with a 100% success rate. This indicates the importance of initial prealignment of the particle pair to the physical surface.

The influence of the downward force (e.g., by a magnetic field gradient that is oriented towards the surface) during the disaggregation process was studied, see Fig. 4(b). Compared to no downward force, we find that a downward force increases the range of initial tilt angles for which disaggregation is successful. Remarkably, in the absence of a downward force, it is found that particles may still successfully separate if the initial tilt angle of the cluster is less than ~9°. Looking at this case in more detail, we find that the simulation time plays an important role. For small angles, the time that it takes to reform a cluster is found to be (much) larger than 10 s (see Ref. [30]), and it is found to increase exponentially as the initial tilt angle approaches zero. From this, we conclude that a downward force, e.g., due to a magnetic field gradient or gravity, is not strictly necessary but can be used to increase the effectiveness of cluster disaggregation.

To study the role of the hydrodynamic interactions in the disaggregation process, data were generated for the case that the hydrodynamic interaction between the particles and/or to the surface was switched off. As shown in Fig. 4(c), the hydrodynamic interaction between the particles decreases the range of initial tilt angles for which successful particle separation is achieved by a few degrees. This is a consequence of the two particles moving away from each other and each particle tending to drag along the other particle due to the surrounding viscous fluid. The hydrodynamic interaction to the surface is found to increase the probability of separation, which is due to the additional drag which reduces the lifting motion from the surface that occurs when particles reform into a cluster.

For a more analytical understanding of the simulated particle dynamics, we derived equations for the radial and vertical components of the particle velocity from the force balance as discussed in detail in Ref. [30]. In particular, we neglect hydrodynamic interactions between the particles and gravity [30] to obtain an analytical equation for the relative movement direction angle α_v with respect to the surface at small initial tilt angles (α),

$$\alpha_v|_{\text{small}\,\alpha} \cong \tan\ \alpha_v = \frac{v_z}{v_{r_h}} = \frac{\gamma^{||}[(1-5\ \sin^2\alpha)\sin\ \alpha + 2\ \sin\ \alpha] - \frac{4\pi r^4}{3\mu_0 m}\left|\frac{\partial B}{\partial z}\right|}{2\gamma^{\perp}(1-5\ \sin^2\alpha)\cos\ \alpha}, \tag{8}$$

in which v_z and v_{r_h}, respectively, are the relative out-of-plane and in-plane velocity components of the particles with respect to the surface. The factors $\gamma^{\perp}$ and $\gamma^{||}$ account for the additional hydrodynamic drag on the particle when moving orthogonal or parallel to the nearby surface [25]. Inspecting Eq. (8) to obtain particle separation, first of all, the in-plane velocity component v_{r_h} needs to be positive (corresponding to separation of the particles), which is according to Eq. (8) only the case when the initial tilt angle is less than $|\alpha_0| \leq \sin^{-1}(0.2^{0.5}) \cong 26.6°$. However, starting out within this range, particles may still reach vertical alignment when the relative movement direction angle α_v is larger than this threshold angle and causes the relative particle angle α after a while to become larger than the threshold angle of ~26.6°. In order to reach successful separation, this critical angle should not be crossed. Due to the nonlinearity of the equation, it is too difficult to derive a simple analytical criterion that meets this requirement. However, a less strong, but still correct, criterion to achieve particle separation is that, besides $|\alpha| \leq \sin^{-1}(0.2^{0.5})$, the relative movement direction angle α_v needs to be smaller than or equal to the relative particle angle, i.e., $\alpha_v \leq \alpha_0$. Meeting this requirement implies that the relative particle angle stays constant or decreases as the particle moves $\alpha|_{t>0} \leqslant \alpha_0$. As a result, the horizontal velocity component remains positive, leading to successful separation. Using Eq. (8), assuming small α_0 and inserting the parameter values of the M-270 particles, an analytical criterion is obtained for the initial particle angle,

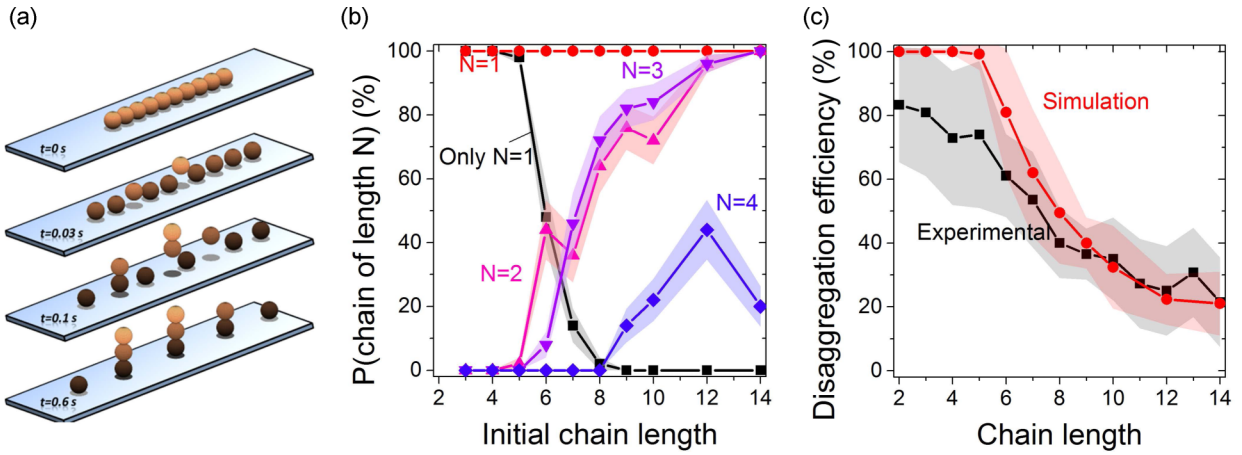

FIG. 5. (Color online) Disaggregation of magnetic particle chains at a physical surface. (a) Snapshots of the simulated disaggregation of a ten-particle chain. The disaggregation protocol leads to single particles and short chains oriented along the surface normal. (b) Probability to obtain chains oriented along the surface normal with N particles after 10 s of application of a magnetic field along the surface normal ($\mathbf{B} = 15\,\mathrm{mT}\,\hat{\mathbf{e}}_z$; $|\mathbf{F}_{\mathrm{down}}| = 0.26$ pN). For each initial chain size, 50 simulations were carried out. The standard error of the mean is represented by the shaded area. The black squares correspond to the probability to completely disaggregate a chain into separate single particles (i.e., after 10 s, all remaining clusters have a chain length of 1). The percentages do not add up to 100% because, in a single simulation, chains of different lengths may be obtained, e.g., $N = 1$–3 [see panel (a)]. (c) Comparison of the disaggregation efficiency as found in simulation and in experiment. Experimental data points correspond to at least four measured chains, i.e., for smaller chains, more measurements (e.g., 20 two-particle clusters) were performed.

i.e.,

$$\alpha_0 \leqslant \sqrt[3]{\frac{4\pi(2R)^4}{30\mu_0 m}\left|\frac{\partial B}{\partial z}\right|} \cong 5.6^\circ. \tag{9}$$

Important to note is that it is assumed that the ratio of the hydrodynamic correction factors $\gamma^{\perp}/\gamma^{||}$ is $\sim$1.5. This is approximately correct at a particle center distance from the surface $\leq 2R$. In particular, for shorter distances, this ratio is slightly larger than 1.5, which would result in a higher estimate of the initial particle angle. Furthermore, from simulations, it is found that two-particle clusters that successfully separate do not reach such relative heights.

Compared to our computations [see Fig. 3(a)], the estimated initial tilt angle for which separation should occur is smaller by roughly a factor of 2. The reason for this difference is that, for initial tilt angles above the estimated value, separation might still be obtained, even if $\alpha_v \leqslant \alpha_0$ does not hold. For example, at a starting angle of $\alpha_0 \sim 12^\circ$, initially, the relative movement direction angle is larger than the relative particle angle. This causes an initial increase in the relative particle angle, but before the relative particle angle has reached the threshold, i.e., $|\alpha| = \sin^{-1}(0.2^{0.5}) \cong 27^\circ$, the requirement of $\alpha_v \leqslant \alpha$ is met due to the increasing influence of the field gradient towards the surface at longer distances. As a consequence, the threshold angle will not be exceeded, and both particles will still separate as found from simulations [as shown in Fig. 3(a)].

Interestingly, we find that the surface drag correction factors have a significant influence on the maximum initial relative particle angle that still allows for separation. For example, in case $\gamma^{||} = 1 = \gamma^{\perp}$, the analytical calculation would have led to a maximum angle of $\alpha_0 = 0.6^\circ$, which is nearly tenfold smaller. Since the surface-caused increase in hydrodynamic drag on the particles is larger in the vertical direction ($\gamma^{\perp} > \gamma^{||}$), the vertical movement velocity is reduced more than the horizontal velocity, which results in a larger initial tilt angle for which particles may successfully separate. Consequently, the nearby surface does not only affect particle separation by inhibiting the out-of-plane motion of one of the two particles, but also affects particle separation by slowing down the out-of-plane motion of the other particle with respect to the in-plane motion.

From the numerical and analytical studies of the separation dynamics of two-particle clusters in a magnetic field, we conclude that an initial misalignment of the cluster with respect to the surface is most detrimental to the separation probability. In practice, a good alignment may be achieved by applying a horizontally oriented field prior to the vertical field component. This is even more important when smaller particles are used; due to Brownian motion, precise alignment with the surface becomes more difficult, which can be solved by applying higher field strengths and stronger field gradients towards the surface. Initial alignment can still be frustrated by strong variations in particle size or a large surface roughness of the particles, so particles are preferred with a spherical shape and a narrow size distribution.

C. Disaggregation of multiparticle clusters

In addition to two-particle clusters, we numerically simulated the disaggregation of clusters consisting of more than two particles. For the same number of particles, different cluster configurations are possible in principle: (i) one-dimensional (1D) clusters, i.e., chains, (ii) two-dimensional (2D) clusters, i.e., sheets, and (iii) three-dimensional (3D) clusters. In the simulations, only chain- and sheetlike clusters were considered. Three-dimensional clusters were not considered because of computational time costs due to the large number of particles. Experimentally, it was found that the repeated application of the surface alignment steps and the disaggregation steps gradually breaks down the clusters from 3D clusters

to 2D clusters and finally to single particles [8]. The results presented here on the disaggregation of 2D clusters, therefore, apply partially to the disaggregation of 3D clusters. In the paper by Straube *et al.* [33], initial particle arrangements were programmed using optical traps, and pattern formation was studied in single disaggregation processes. Here, we study single and repeated magnetic disaggregation processes of particle clusters, using magnetic fields to form the initial particle arrangements. Experiments were performed with 2.8 μm Dynal M-270 particles (carboxylated), which are easy to optically track because they stay within the optical focus of the microscope due to the weak Brownian motion.

First, we consider the disaggregation of chainlike magnetic particle clusters. Figure 5(a) shows the typical results from a simulation; snapshots are shown of the simulated disaggregation of a ten-particle chain. Data on different chain lengths were processed, and we determined the disaggregation effectiveness by calculating the probability that (smaller) particle chains with length N remain after application of the magnetic field, see Fig. 5(b). It is found that, for chains containing more than six particles, complete disaggregation occurs less frequently and smaller chains ($N = 2$–4) remain. In practice, these smaller chains can be disaggregated further by first realigning the chains at the surface and, subsequently, reapplying the magnetic field along the surface normal.

Although chains containing more than six particles occasionally are not completely disaggregated after a single application of the magnetic field, partial disaggregation is still achieved. This partial disaggregation may be expressed as a disaggregation efficiency, i.e., the number of obtained single particles divided by the number of particles in the initial chain. In Fig. 5(c), this disaggregation efficiency is plotted and is compared to experimentally gathered data (on the same particles and maintaining the same properties of the external field). It is found that, for short chains, the simulations show a complete disaggregation, whereas in experiments disaggregation efficiencies were obtained of about 75%. For longer chain lengths, the simulated efficiency is similar to the experimental efficiency. Possible causes for this difference are variations in particle size or magnetic content but also a misalignment of the chains with respect to the surface. Variations in particle size or magnetic content might influence disaggregation less in the case of longer chains. Furthermore, misalignment of the chains with the surface is likely for short chains (e.g., due to Brownian motion), but for longer chains, this will be less due to the larger size, which makes Brownian motion slower.

Finally, we consider the disaggregation of two-dimensional particle clusters, i.e., sheetlike formations. Although many different types of configurations are possible for a certain number of particles within the cluster, we chose to simulate only closely packed and highly symmetric configurations. In Fig. 6(a), snapshots are shown of the simulation of a 19-particle cluster, configured in a closely packed hexagon. Figure 6(b) shows the probability of obtaining a certain chain length after application of the magnetic field for configurations as are depicted in the graph. As can be seen, only for large particle clusters containing more than ~14 particles, we find a significant probability to incompletely disaggregate sheetlike clusters. The disaggregation efficiency [see Fig. 6(c)] is also found to be high compared to chain simulations with the same number of particles.

An insightful way to compare sheetlike clusters to chainlike clusters is by comparing the longest chain length present within the cluster. For example, in the case of a sheetlike cluster containing 14 particles, the longest chain length is four particles [see drawing in Fig. 6(b)]. For this particular cluster, we find a probability of about 0.25 to obtain a two-particle chain after the application of the magnetic field, whereas for a chainlike cluster consisting of four particles, this probability is almost zero [see Fig. 5(b)]. The presence of more particles on the side of the chain apparently reduces the disaggregation efficiency. This can be understood as, for a four-particle chain within a sheetlike cluster, the additional neighboring particles contribute all to the component of the dipole force along the surface normal [see Eq. (2)], which will result in

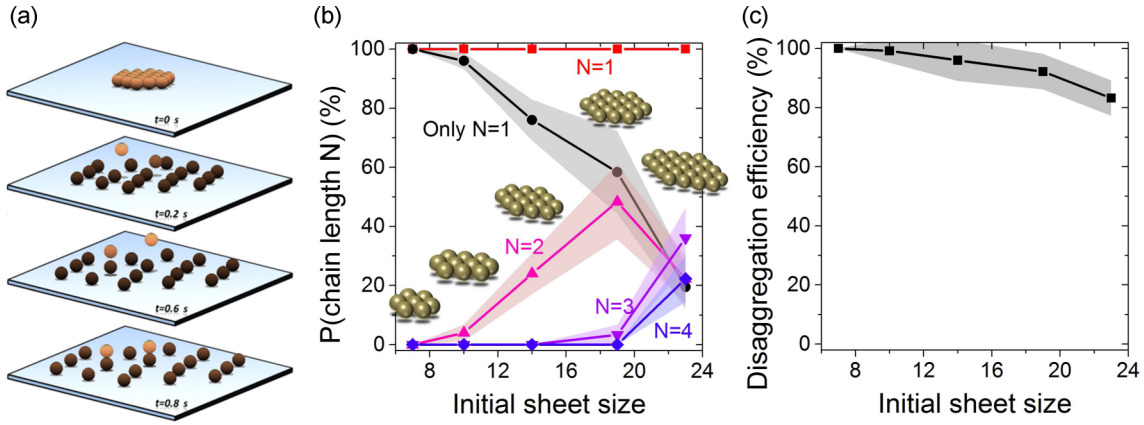

FIG. 6. (Color online) Disaggregation of sheetlike magnetic particle clusters at a physical surface. (a) Snapshots of the simulated disaggregation of a 19-particle sheetlike cluster. Besides obtaining single particles, smaller chains oriented along the surface normal are also obtained. (b) Probability to obtain chains with N particles oriented along the surface normal after 10 s of application of a magnetic field along the surface normal ($\mathbf{B} = 15\,\mathrm{mT}\,\hat{\mathbf{e}}_z$; $|\mathrm{F}_{\mathrm{down}}| = 0.26$ pN). For each initial sheet size, 50 simulations were carried out. The standard error of the mean is represented by the shaded area. The black squares indicate the probability to completely disaggregate a sheetlike cluster into single particles. (c) Disaggregation efficiency computed from the simulation data.

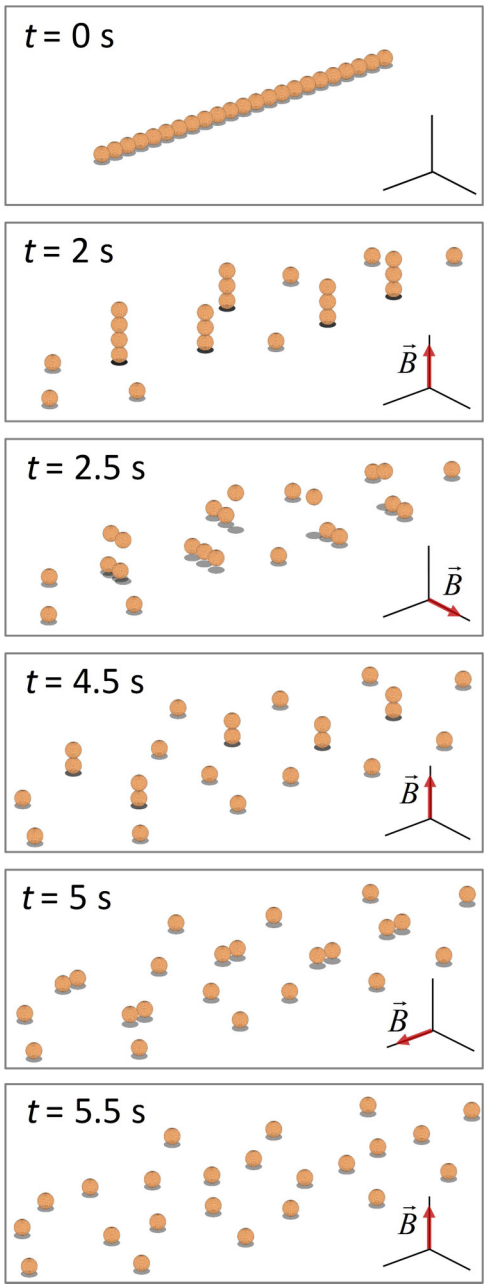

FIG. 7. (Color online) Simulation of the disaggregation of a particle chain consisting of 23 particles by alternatingly applying an in-plane field (5 mT for 0.5 s) and an out-of-plane field (15 mT for 2 s) with respect to the surface, to align the (fragmented) chains to the surface and to disaggregate the chains into smaller chain fragments or separated particles, respectively. To keep the particles near the surface, a downward force of 0.26 pN was applied on each particle, corresponding to the sum of a field gradient force ($-2.8\,\mathrm{T/m}\,\hat{\mathbf{e}}_z$ and 0.22 pN) and a buoyancy force (0.04 pN).

a faster increase in the height difference between particles when a small height difference occurs, e.g., due to Brownian motion. Furthermore, for the completely surrounded particles, the in-plane component of the dipole force is, for a large part, canceled out, reducing the velocity with which the particles separate. In view of Eq. (8), the relative movement direction angle with respect to other particles increases more rapidly due to the stronger vertical and weaker horizontal component of the forces acting on the particles. A small difference in height between sheetlike clustered particles will, therefore, sooner lead to vertical rejoining of the particles.

Nevertheless, comparing different cluster configurations in terms of the total number of clustered particles, sheetlike structures lead to a better separation than chainlike structures. This can be understood as follows. Consider the case of seven particles, clustered in a chainlike structure. When applying the magnetic field along the surface normal, the in-plane force acting on the centered particles is inhibited strongly. For the five centered particles, the repulsive dipole-dipole interaction with the nearest neighbors is canceled out. Only more distant neighbors induce a net displacement, but the resulting force is much weaker as it depends on the fourth power of the radial distance. Consequently, the time to reach sufficient separation to prevent any realignment is relatively long. On the other hand, in case the seven particles are structured in a hexagonal sheetlike structure, only the horizontal displacement of the centered particle is inhibited, but the other particles experience the repulsive interaction of three neighboring particles. Therefore, the time to reach sufficient separation will be much shorter for sheetlike clusters as compared to chainlike clusters.

It is interesting to note that, for all cluster configurations, the induced dipole-dipole interaction will always result in one but often more individual particles. This indicates that the repeated application of a field along the surface normal should, in principle, result in the complete disaggregation of magnetic particle clusters. We, therefore, performed a simulation in which we alternatingly apply an in-plane and an out-of-plane magnetic field to a particle chain consisting of 23 particles. The snapshots in Fig. 7 show that, indeed, the application of such an actuation protocol can lead to complete disaggregation of the particle chain within less than 10 s. Important, however, in this protocol is that the part in which the particles are realigned in plane is shorter or weaker compared to the part in which disaggregation is induced. This is because the magnetic dipole-dipole force for particles with magnetic moments aligned in plane is twice as large compared to particles with equal magnetic moments aligned out-of-plane [see Eq. (2)]. For effective disaggregation, the in-plane alignment step should not undo the achieved particle separation but should only realign the out-of-plane oriented chains to make further disaggregation possible.

V. CONCLUSIONS

To summarize, we have developed a numerical model to simulate the Brownian dynamics of ensembles of magnetic particles in a viscous fluid. To validate the model, it was applied to study the dynamics of magnetic field-based disaggregation of superparamagnetic particle clusters near a surface. Disaggregation is achieved by inducing repulsive magnetic dipole-dipole interaction forces between the particles aligned at a surface. Numerical simulation results were compared to experimental data as a function of magnetic field properties, particle size, cluster size, and cluster geometry. In the case of two-particle clusters, we find that the probability to disaggregate the cluster is strongly determined by the degree of alignment of the cluster with the surface at the instant when the

repulsive interaction is induced. The degree of alignment for which separation is achieved is found to depend on: (i) the size of the particles as this determines the Brownian motion, (ii) the magnetization properties of the particles, (iii) the strength of the field gradient towards the surface, and (iv) the application time of the magnetic field. Typical angles with respect to the surface for which separation is achieved are on the order of 10°–15°.

The probability to reach complete cluster disaggregation scales down with cluster size and depends strongly on the cluster configuration. In particular, sheetlike clusters disaggregate more effectively than chainlike clusters containing the same number of particles. A linear configuration (1D) has two limiting effects with respect to a sheetlike configuration (2D) with the same number of particles, namely: (i) a steric hindrance for particle motion towards the cluster extremities for more particles due to the reduced dimensionality and (ii) lower repulsive dipole-dipole forces because, on average, the particles have fewer nearest neighbors. The insights obtained from the numerical simulations will help to improve magnetic field-based disaggregation and dispersion of magnetic particles in microfluidic applications. The disaggregation method opens new possibilities for magnetic particle-based lab-on-chip applications. For example, the method may be applied to undo magnetic clustering effects that may have occurred in magnetic actuation steps, such as for fluid mixing and target capturing. Also, a disaggregation step can reset the particle distribution for subsequent labeling or detection steps.

Most importantly, the method presented in this paper to numerically simulate multiparticle dynamics has a very general applicability for particle-based biotechnological assays because such assays are always performed using ensembles of many particles. Examples of assay processes that can be studied and can be optimized by the simulation methodology are surface-binding assays [4], agglutination assays [3,11], methods to perform magnetic washing or apply stringency to particles at a biosensor surface [4,6,12], and technologies for particle-based target purification and enrichment [10,14]. Simulation results give detailed insight into the fundamental dynamics of magnetic particles, allow for a more in-depth interpretation of experimental data, and give new ideas on how assays can be controlled and can be used. We expect that the numerical simulation of multiparticle dynamics will be broadly applied and will be very useful for the further development of magnetic particle-based bionanotechnologies.

ACKNOWLEDGMENTS

This project was funded by the Dutch Technology Foundation (STW) under Grant No. 10458.

[1] A. van Reenen, A. M. de Jong, J. M. J. den Toonder, and M. W. J. Prins, Lab Chip (2014), doi:10.1039/C3LC51454D.
[2] M. A. Gijs, F. Lacharme, and U. Lehmann, Chem. Rev. **110**, 1518 (2010).
[3] A. Ranzoni, G. Sabatte, L. J. van IJzendoorn, and M. W. J. Prins, ACS Nano **6**, 3134 (2012).
[4] D. M. Bruls *et al.*, Lab Chip **9**, 3504 (2009).
[5] J. M. Nam, C. S. Thaxton, and C. A. Mirkin, Science **301**, 1884 (2003).
[6] I. De Vlaminck and C. Dekker, Annu. Rev. Biophys. **41**, 453 (2012).
[7] J. Lipfert, J. W. Kerssemakers, T. Jager, and N. H. Dekker, Nat. Methods **7**, 977 (2010).
[8] Y. Gao, A. van Reenen, M. A. Hulsen, A. M. de Jong, M. W. J. Prins, and J. M. J. den Toonder, Lab Chip **13**, 1394 (2013).
[9] Y. Gao, A. van Reenen, M. A. Hulsen, A. M. de Jong, M. W. J. Prins, and J. M. J. den Toonder, Microfluid. Nanofluid. **16**, 265 (2014).
[10] R. C. den Dulk, K. A. Schmidt, G. Sabatte, S. Liebana, and M. W. J. Prins, Lab Chip **13**, 106 (2013).
[11] Y. Moser, T. Lehnert, and M. A. M. Gijs, Lab Chip **9**, 3261 (2009).
[12] A. Jacob, L. J. van IJzendoorn, A. M. de Jong, and M. W. J. Prins, Anal. Chem. **84**, 9287 (2012).
[13] A. H. Ng, K. Choi, R. P. Luoma, J. M. Robinson, and A. R. Wheeler, Anal. Chem. **84**, 8805 (2012).
[14] R. Gottheil, N. Baur, H. Becker, G. Link, D. Maier, N. Schneiderhan-Marra, and M. Stelzle, Biomed Microdevices **16**, 163 (2014).
[15] S. Melle, O. G. Calderón, M. A. Rubio, and G. G. Fuller, Phys. Rev. E **68**, 041503 (2003).
[16] W. Zylka and H. C. Ottinger, J. Chem. Phys. **90**, 474 (1989).
[17] X. J. A. Janssen, A. van Reenen, L. J. van IJzendoorn, and M. W. J. Prins, Colloids Surf., A **373**, 88 (2011).
[18] K. van Ommering, C. C. H. Lamers, J. H. Nieuwenhuis, L. J. van IJzendoorn, and M. W. J. Prins, J. Appl. Phys. **105**, 104905 (2009).
[19] R. J. S. Derks, A. J. H. Frijns, M. W. J. Prins, and A. Dietzel, Microfluid. Nanofluid. **9**, 357 (2010).
[20] S. S. Shevkoplyas, A. C. Siegel, R. M. Westervelt, M. G. Prentiss, and G. M. Whitesides, Lab Chip **7**, 1294 (2007).
[21] H. C. Tekin, M. Cornaglia, and M. A. M. Gijs, Lab Chip **13**, 1053 (2013).
[22] D. L. Ermak and J. A. McCammon, J. Chem. Phys. **69**, 1352 (1978).
[23] R. R. Schmidt, J. G. Cifre, and J. G. de la Torre, J. Chem. Phys. **135**, 084116 (2011).
[24] Y. von Hansen, M. Hinczewski, and R. R. Netz, J. Chem. Phys. **134**, 235102 (2011).
[25] J. Leach, H. Mushfique, S. Keen, R. Di Leonardo, G. Ruocco, J. M. Cooper, and M. J. Padgett, Phys. Rev. E **79**, 026301 (2009).
[26] H. Brenner, Chem. Eng. Sci. **16**, 242 (1961).
[27] A. J. Goldman, R. G. Cox, and H. Brenner, Chem. Eng. Sci. **22**, 637 (1967).
[28] P. S. Grassia, E. J. Hinch, and L. C. Nitsche, J. Fluid Mech. **282**, 373 (1995).
[29] S. Krishnamurthy, A. Yadav, P. E. Phelan, R. Calhoun, A. K. Vuppu, A. A. Garcia, and M. A. Hayes, Microfluid. Nanofluid. **5**, 33 (2008).
[30] See Supplemental Material at http://link.aps.org/supplemental/10.1103/PhysRevE.89.042306 for the influence of gravitational

forces compared to magnetic gradient forces, the error analysis of the numerical scheme, the error analysis for the excluded volume force, the simulated time to reach cluster reformation for different initial tilt angles, the breaking of two-particle clusters in the absence of a field gradient, and a derivation of the relative movement direction angle in the disaggregation of two-particle clusters.

[31] Y. Gao, M. A. Hulsen, T. G. Kang, and J. M. J. den Toonder, Phys. Rev. E **86**, 041503 (2012).

[32] A. van Reenen, Y. Gao, A. H. Bos, A. M. de Jong, M. A. Hulsen, J. M. J. den Toonder, and M. W. J. Prins, Appl. Phys. Lett. **103**, 043704 (2013).

[33] A. V. Straube, A. A. Loius, J. Baumgartl, C. Bechinger, and R. P. A. Dullens, Europhys. Lett. **94**, 48008 (2011).